

# Wear behavior and self tribofilm formation of hot-pressed $\text{Al}_2\text{O}_3/\text{TiC}/\text{CaF}_2$ ceramic composites sliding against cemented carbide

Deng Jianxin\*, Cao Tongkun, Yang Xuefeng, Liu Jianhua, Sun Junlong, Zhao Jinlong

*Department of Mechanical Engineering, Shandong University, Jinan 250061, Shandong Province, PR China*

Received 23 June 2005; received in revised form 21 July 2005; accepted 1 September 2005

Available online 22 December 2005

## Abstract

$\text{Al}_2\text{O}_3/\text{TiC}$  ceramic composites with the additions of  $\text{CaF}_2$  solid lubricants were produced by hot pressing. Sliding wear tests against cemented carbide were performed on these ceramic composites using the ring-block method. The friction coefficient and wear rates were measured. Results showed that the friction coefficient and the specific wear rate decreased with the increase of  $\text{CaF}_2$  content up to 10 vol.%, with further increases in  $\text{CaF}_2$  content, both the friction coefficient and the wear rate increased rapidly. SEM observations showed that self tribofilms were consistently formed on the wear surfaces. Two types of tribofilms are present on the worn surface depending on the  $\text{CaF}_2$  content. A dense self tribofilm with a smooth surface associated with small friction coefficient and low wear rate was formed by the releasing and smearing of  $\text{CaF}_2$  solid lubricants on the wear surface when with low  $\text{CaF}_2$  content (less than 10 vol.%). This dense self tribofilm acted as solid lubricant film between the sliding couple, protected the ceramics from severe wear by brittle microfracture, and thus significantly reduced the friction coefficient and the wear rate. A broken tribofilm associated with high friction coefficient and large wear rate was formed when with high  $\text{CaF}_2$  content (more than 10 vol.%). The reason is that large degradation of mechanical properties occurred in samples with high  $\text{CaF}_2$  contents.

© 2005 Elsevier Ltd and Techna Group S.r.l. All rights reserved.

**Keywords:** B. Composites; C. Wear resistance; D.  $\text{Al}_2\text{O}_3$ ; Self-lubrication

## 1. Introduction

Advanced ceramic materials exhibit high hardness, high stiffness, excellent chemical and mechanical stability, which make them promising candidates for wear-resistance components. They have excellent prospects for tribological applications especially under severe conditions. Nowadays advanced ceramics are widely used in cutting tools, dies for drawing or extrusion, seal rings, valve seats, bearing parts, and a variety of high temperature engine parts, etc. [1–3]. Consequently, clarification of wear behaviors of ceramic materials has received much attention over the last two decades.

It is well known that the friction coefficient of  $\text{Al}_2\text{O}_3$  based ceramic composites under dry sliding conditions is relative high [4–6]. Sometime, these properties render this ceramic composite inappropriate for practical applications. Therefore,

considerable effort has been made to improve the tribological performance of ceramic composites. Several researchers [7–12] have found that the incorporation of solid lubricants in the ceramic matrix to develop the self-lubricating ceramic composites can improve their tribological properties. Self-lubricating ceramic composites, consisting of a supporting ceramic matrix surrounding dispersed pockets of one or more softer lubricating species, have been used in a wide range of high temperature tribological applications.

$\text{CaF}_2$  is a well known and widely used solid lubricant. It has physical (i.e. it prevents adhesion), chemical (i.e. it enables tribo-chemical reactions) and microstructural (i.e. it has a lamellar structure with low shear strength) influences on the tribological contact of working surfaces. The mechanism behind their effective lubricating performance is understood to be owing to easy shearing along the basal plane of the hexagonal crystalline structures. Also they are useful additions in the production of self-lubricating ceramic composites, and are used in different anti-wear applications. In earlier studies [7–12], some of the ceramic composites, such as:  $\text{Al}_2\text{O}_3/\text{CaF}_2$ ,

\* Corresponding author. Tel.: +86 531 88392047

E-mail address: jxdeng@sdu.edu.cn (J. Deng).

Table 1  
Particle size, purity and manufacturer of the starting powders

Starting powder	Average particle size ( $\mu\text{m}$ )	Purity (%)	Manufacture
$\text{Al}_2\text{O}_3$	1–2	>99.9	Zibo aluminum works
TiC	1–2	>99.5	Zhuzhou cemented carbide works
$\text{CaF}_2$	<1	>98.5	Beijing Yili fine chemical products works

$\text{Al}_2\text{O}_3$ /graphite,  $\text{Si}_3\text{N}_4$ /BN, and TZP/graphite, have been developed and used in various applications, mechanical properties and microstructural studies on them have also been extensively carried out. It has been shown that the additions of solid lubricants to the ceramic matrix can improve their tribological properties.

Numerous studies have been conducted on the friction and wear behaviors of self-lubricating ceramics. Most of them have revealed that thin layers, so called tribofilms, are observed on the wear surfaces. Actual wear often occurs at the contact interfaces where a tribofilm is present. Tribofilm might play an important role in the sliding wear behaviors of ceramics. Several researches have addressed the characterization of the tribofilms and their role on the wear behaviors [13–15]. Their results showed that sliding couples that form a stable and adherent film exhibit much less wear rate than couples that do not form a stable and adherent film.

In the present study,  $\text{Al}_2\text{O}_3$ /TiC ceramic composites with additions of  $\text{CaF}_2$  solid lubricants were produced by hot pressing. The effect of the solid lubricants on the micro-structure, mechanical properties, and tribological behaviors of this ceramic composite has been studied. Detailed observations and analyses have been conducted to clarify the formation mechanism of the self tribofilms and their effects on the friction and wear behavior of these ceramic composites.

## 2. Experimental procedure

### 2.1. Materials and processing

The starting powders used to fabricate the ceramic composites are listed in Table 1 with their particle sizes, purities and manufacturers.  $\text{Al}_2\text{O}_3$ /TiC (volume ratio 1:1) was used as the baseline material. Additions of  $\text{CaF}_2$  solid lubricant particles were added to  $\text{Al}_2\text{O}_3$ /TiC matrix. The range of solid lubricant additions to the  $\text{Al}_2\text{O}_3$ /TiC matrix was from 0 to 15 vol.% as listed in Table 2.

Table 2  
Compositions and mechanical properties of hot pressed  $\text{Al}_2\text{O}_3$ /TiC/ $\text{CaF}_2$  ceramic composites

Specimen	Compositions (vol.%) (volume ratio: $\text{Al}_2\text{O}_3$ :TiC = 1:1)	Flexural strength (MPa)	Hardness (GPa)	Fracture toughness ( $\text{MPa m}^{1/2}$ )
AT	$\text{Al}_2\text{O}_3$ + TiC	$800 \pm 43$	$20.0 \pm 0.6$	$5.2 \pm 0.3$
ATF1	$\text{Al}_2\text{O}_3$ + TiC + 5% $\text{CaF}_2$	$478 \pm 32$	$13.2 \pm 0.8$	$3.4 \pm 0.2$
ATF2	$\text{Al}_2\text{O}_3$ + TiC + 10% $\text{CaF}_2$	$590 \pm 29$	$15.3 \pm 0.7$	$3.6 \pm 0.3$
ATF3	$\text{Al}_2\text{O}_3$ + TiC + 15% $\text{CaF}_2$	$418 \pm 33$	$9.6 \pm 0.5$	$3.3 \pm 0.3$

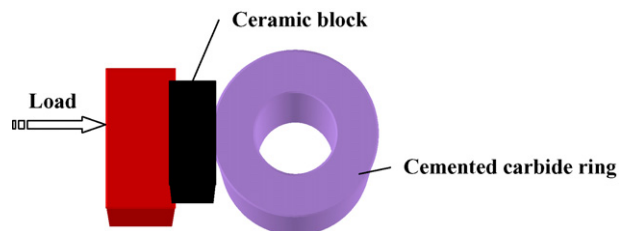


Fig. 1. Schematic diagram of the friction and wear test apparatus (dimension: ceramic block  $15 \text{ mm} \times 12 \text{ mm} \times 5 \text{ mm}$ , cemented carbide ring specimen  $\text{Ø}50 \text{ mm} \times \text{Ø}35 \text{ mm} \times 15 \text{ mm}$ ).

The combined powders were prepared by wet ball milling in alcohol for 60 h with cemented carbide balls. Following drying, the final densification of the combined powders was accomplished by hot pressing with a pressure of 32 MPa in argon atmosphere for 15 min to produce a ceramic disk. The sintering temperature employed for hot pressing was  $1700^\circ\text{C}$ .

### 2.2. Material characterization

Test pieces of  $3 \text{ mm} \times 4 \text{ mm} \times 36 \text{ mm}$  in dimension were prepared from the disk by cutting and grinding using a diamond wheel and were offered for measurement of flexural strength, Vickers hardness and fracture toughness. Three-point-bending mode was used to measure the flexural strength over a 30 mm span at a crosshead speed of  $0.5 \text{ mm/min}$ . Fracture toughness measurement was performed using indentation method in a hardness tester (ZWICK3212) using the formula proposed by Cook and Lawn [16]. On the same apparatus the Vickers hardness was measured on polished surface with a load of 98 N. Data for hardness, flexural strength, and fracture toughness were gathered on five specimens and averaged.

### 2.3. Friction and wear tests

Friction and wear tests were conducted with a MRH-3 high-speed ring-block tribometer. The schematic diagram of this equipment is shown in Fig. 1. The block specimen ( $15 \text{ mm} \times 12 \text{ mm} \times 5 \text{ mm}$ ) was made of ceramic materials having a polished surface with a surface roughness of  $0.08 \mu\text{m}$ . The ring specimen ( $\text{Ø}50 \text{ mm} \times \text{Ø}35 \text{ mm} \times 15 \text{ mm}$ ) was made of YG8 (WC + 8 vol.% Co) cemented carbide with a hardness of HRA 89. The ring surface was polished to produce a final surface roughness of  $0.05 \mu\text{m}$ . Both the block and the ring were rinsed with hexane, and then ultrasonically cleaned in fresh hexane, followed by ultrasonic cleaning with acetone. The ceramic

block is fixed, while the cemented carbide ring is rotated with a speed of 200–600 r/min. A normal load of 70 N was applied in all the tests. Each test was run over a period of 10 min. The friction coefficient was calculated by dividing the measured tangential force by the applied normal force. The mass loss of the worn ceramic blocks was measured with an accurate electron balance (minimum 0.001 mg). The wear rate  $W$  [17] is defined as the volume loss,  $V$ , divided by the applied normal load,  $P$ , times the sliding distance,  $L$ .

$$W = \frac{V}{PL} \quad (1)$$

where the  $W$  has the units of volume loss per unit force per unit distance ( $\text{mm}^3/\text{N m}$ ).

XRD (D/max-2400) analysis was undertaken to identify the crystal phases present after sintering. The microstructures of sintered materials and the worn regions of the ceramic blocks were examined using scanning electron microscopy (HITACH S-570).

### 3. Results and discussion

#### 3.1. Microstructure and mechanical properties

The mechanical properties of  $\text{Al}_2\text{O}_3/\text{TiC}/\text{CaF}_2$  ceramic composites with different content of  $\text{CaF}_2$  solid lubricants are listed in Table 2. It can be seen that additions of  $\text{CaF}_2$  solid lubricants to the  $\text{Al}_2\text{O}_3/\text{TiC}$  matrix led to a decrease in the flexural strength, fracture toughness, and hardness compared to a normal  $\text{Al}_2\text{O}_3/\text{TiC}$  composite. The flexural strength of  $\text{Al}_2\text{O}_3/\text{TiC}$  composite with 10 vol.%  $\text{CaF}_2$  exhibited a maximum value of 590 MPa, and with further increasing of  $\text{CaF}_2$  content it showed a downward trend. The trend of the fracture toughness and the hardness is the same as that of the flexural strength. Fig. 2 illustrates the X-ray diffraction analysis of the  $\text{Al}_2\text{O}_3/\text{TiC}/\text{CaF}_2$  ceramic composite after sintering at 1700 °C for 15 min. It can be seen that  $\text{Al}_2\text{O}_3$ , TiC, and  $\text{CaF}_2$  are all existed in the sintered specimens.

The typical microstructure from the polished surface of hot-pressed  $\text{Al}_2\text{O}_3/\text{TiC}/\text{CaF}_2$  ceramic composite is shown in Fig. 3.

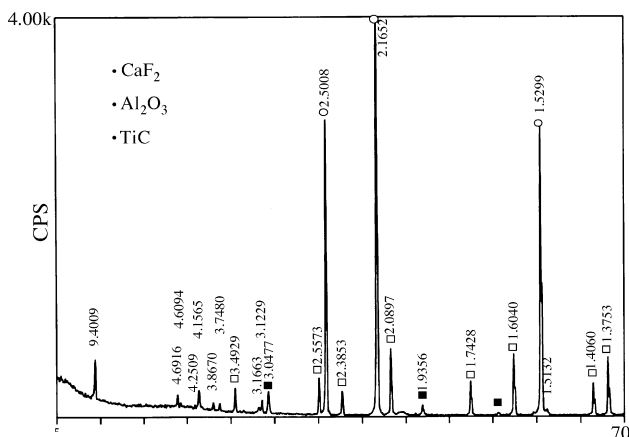


Fig. 2. X-ray diffraction analysis of the  $\text{Al}_2\text{O}_3/\text{TiC}/\text{CaF}_2$  ceramic composite after sintering at 1700.

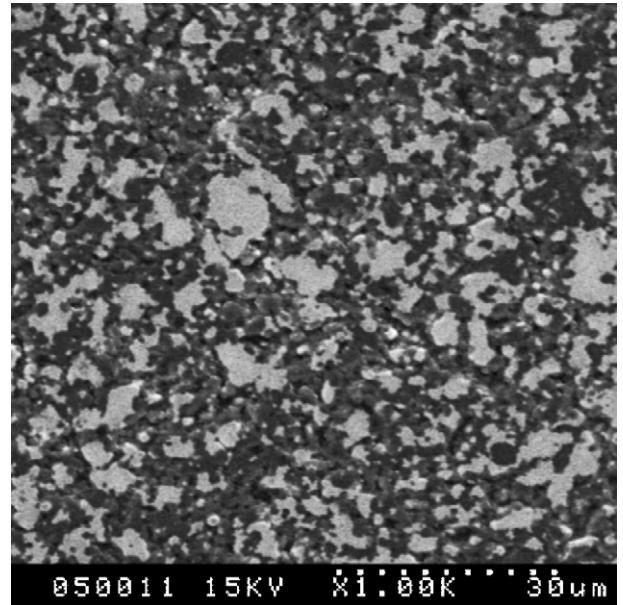


Fig. 3. Typical microstructure of the polished surface of  $\text{Al}_2\text{O}_3/\text{TiC}/\text{CaF}_2$  ceramic composite.

The black areas were identified by EDX analysis as  $\text{Al}_2\text{O}_3$ , and the white phases with clear contrast were TiC and  $\text{CaF}_2$ . It can be seen that the TiC and  $\text{CaF}_2$  particles are quite uniformly distributed throughout the microstructure, porosity is virtually absent, and the solid lubricant phases were uniformly distributed with the matrix with very few second phase agglomerates or matrix-rich regions. Fig. 4 shows the SEM micrograph of the fracture surfaces of  $\text{Al}_2\text{O}_3/\text{TiC}/\text{CaF}_2$  ceramic composite. From this SEM micrograph, different morphologies of the composite can be seen clearly. The  $\text{Al}_2\text{O}_3/\text{TiC}/\text{CaF}_2$  composites exhibited a rough fracture surface, resulting from the mixed transgranular and intergranular fracture modes.

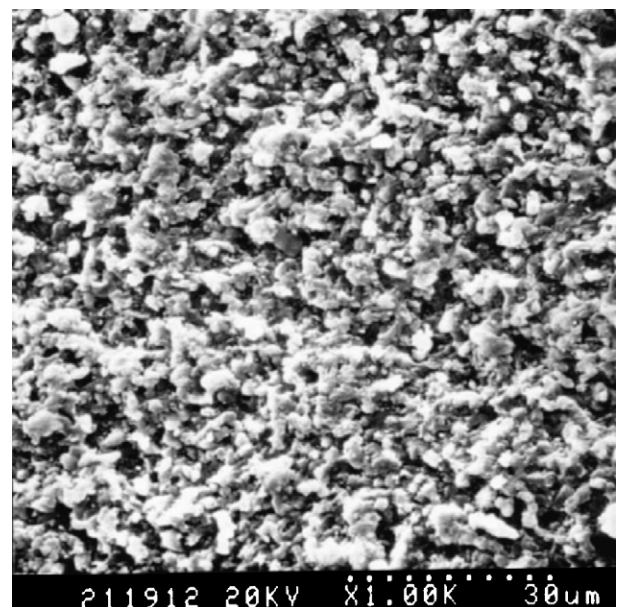


Fig. 4. SEM micrograph of the fracture surface of  $\text{Al}_2\text{O}_3/\text{TiC}/\text{CaF}_2$  ceramic composite.

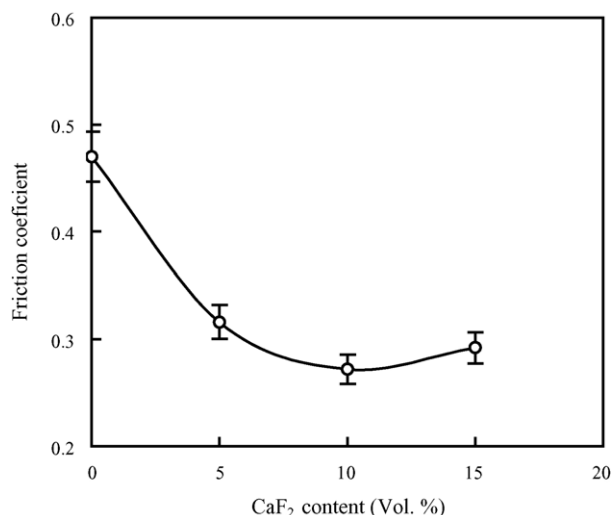


Fig. 5. Effect of the CaF<sub>2</sub> content on the friction coefficient of the Al<sub>2</sub>O<sub>3</sub>/TiC/CaF<sub>2</sub> ceramic composites (sliding speed  $v = 400$  r/min).

### 3.2. Friction coefficient and specific wear rates

The effect of the CaF<sub>2</sub> content on the friction coefficient of the ceramic composite is shown in Fig. 5. It can be seen that the friction coefficient continuously decreased with increases in the CaF<sub>2</sub> content up to 10 vol.%, and decreased from 0.47 for Al<sub>2</sub>O<sub>3</sub>/TiC to 0.27 for Al<sub>2</sub>O<sub>3</sub>/TiC/10 vol.% CaF<sub>2</sub>. With further increasing CaF<sub>2</sub> content the friction coefficient showed a little increase. The ceramic composite without CaF<sub>2</sub> solid lubricants exhibited the highest friction coefficient, while the composite with 10 vol.% CaF<sub>2</sub> solid lubricants showed the smallest friction coefficient under the same test conditions.

Fig. 6 illustrates the effect of the sliding speed on the friction coefficient of the ceramic composite. It is indicated that the friction coefficient showed a downward trend with an increase in the sliding speed. The ceramic composite without CaF<sub>2</sub> solid lubricants exhibited a higher friction coefficient when compared with the composite with CaF<sub>2</sub> under all the test conditions.

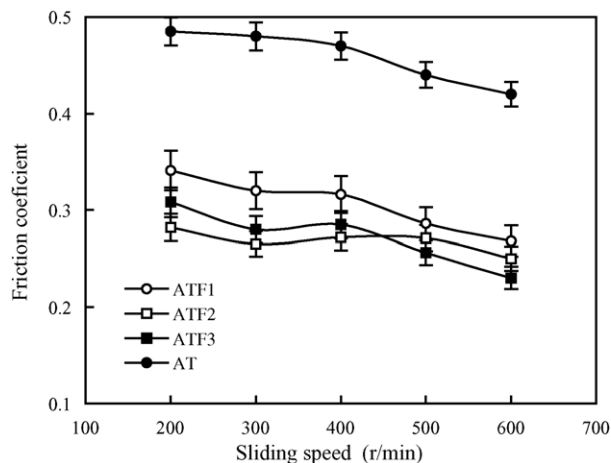


Fig. 6. Effect of the sliding speed on the friction coefficient of the ceramic composites.

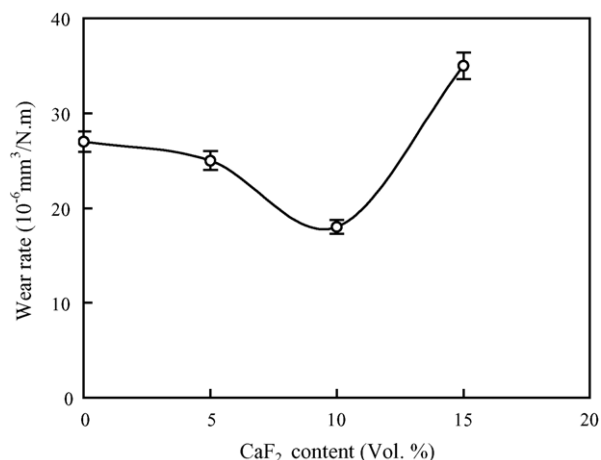


Fig. 7. Effect of the CaF<sub>2</sub> content on the wear rate of the Al<sub>2</sub>O<sub>3</sub>/TiC/CaF<sub>2</sub> ceramic composites (sliding speed  $v = 400$  r/min).

Fig. 7 shows the influence of CaF<sub>2</sub> content on the wear rate of Al<sub>2</sub>O<sub>3</sub>/TiC/CaF<sub>2</sub> composites. It can be seen that when the CaF<sub>2</sub> content is less than 10 vol.%, the wear rate decreases with the increase of CaF<sub>2</sub> content, with further increases in the CaF<sub>2</sub> content, the wear rate of Al<sub>2</sub>O<sub>3</sub>/TiC/CaF<sub>2</sub> increases rapidly.

### 3.3. Wear surface studies

Typical SEM micrograph of the worn surface of Al<sub>2</sub>O<sub>3</sub>/TiC composite without CaF<sub>2</sub> solid lubricants is shown in Fig. 8. There were numerous scratches and pits on the wear surface. The wear track was mangled, and showed a “brushing-off” of debris on the worn surface. Significant surface damage can be observed in the form of a scratched and smeared appearance. This suggests that the primary wear mechanism of Al<sub>2</sub>O<sub>3</sub>/TiC composite is abrasive wear.

Fig. 9(a) and (b) shows the SEM micrographs of the worn surface of ATF2 ceramic composite with 10 vol.% of

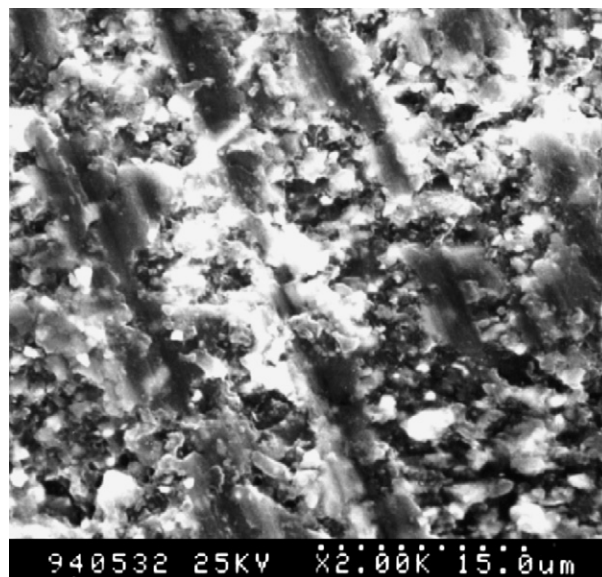


Fig. 8. SEM micrograph of the worn surface of the Al<sub>2</sub>O<sub>3</sub>/TiC composite without CaF<sub>2</sub> solid lubricants (sliding speed  $v = 400$  r/min).



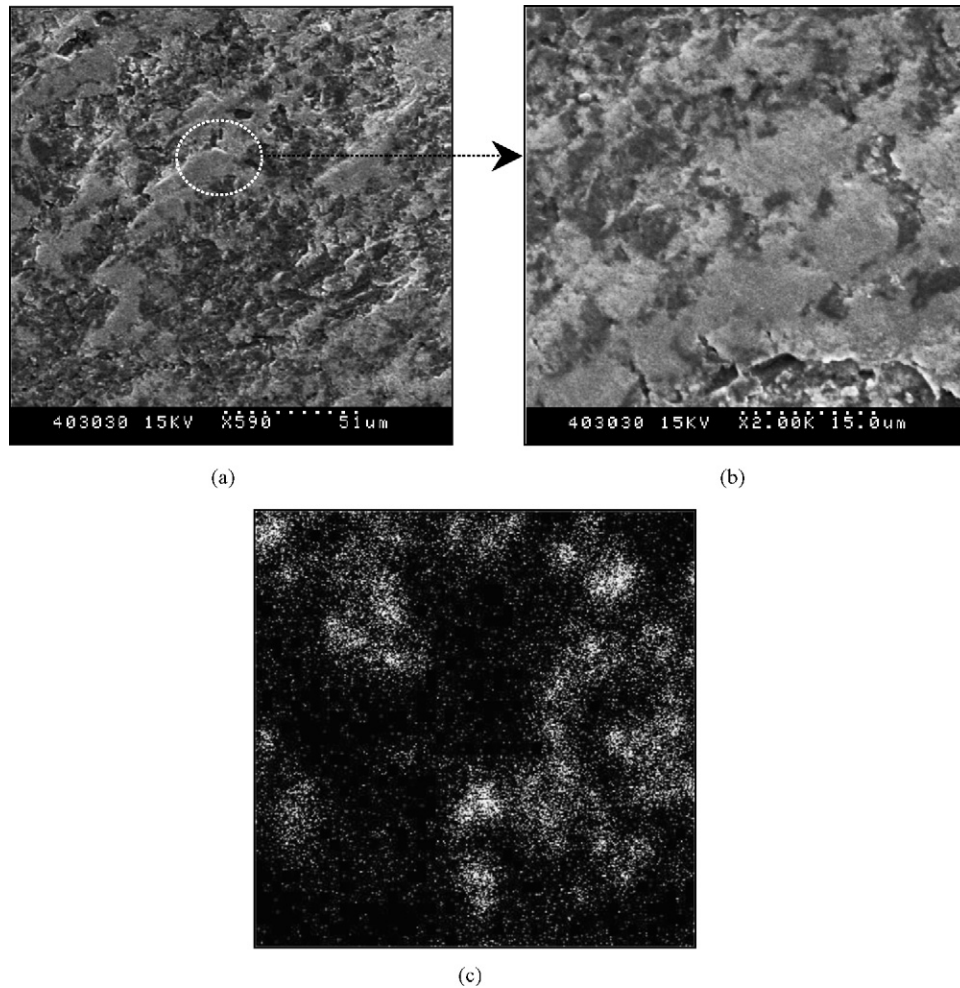


Fig. 9. SEM micrographs of (a) the worn surface of ATF2 ceramic composite, (b) enlarged SEM micrograph corresponding to (a), (c) the F element distribution corresponding to (a) (sliding speed  $v = 400$  r/min).

proportion  $\text{CaF}_2$  solid lubricants. In comparison with Fig. 8, it exhibited a relatively smooth surface, both mechanical plowing grooves and scratches could not be observed, and there is no distinct crack on the wear track. A SEM/EDX map of the distribution of fluorine (i.e. with  $\text{CaF}_2$ ) on the worn surface is shown in Fig. 9(c). The results indicate that  $\text{CaF}_2$  has been released and smeared on the wear surface, and reveals the existence of a thin dense self tribofilm on the worn surface after sliding wear tests. Fig. 10 illustrates the schematic diagram of the formation process of self tribofilm on the wear track.

Fig. 11 shows the stress distribution in the sliding couple (ATF2/YG8) calculated by finite element method (FEM). It was found that the maximum main and shear stresses are at the center of the contact area between the sliding couple. The main stresses exhibited a maximum value of 97 MPa, and the maximum shear stress is of 135 MPa. Comparison of maximum main stress and shear stress of AT and ATF2 ceramic composites sliding against YG8 cemented carbide are listed in Table 3. It can be seen that additions of  $\text{CaF}_2$  solid lubricants to the  $\text{Al}_2\text{O}_3/\text{TiC}$  matrix led to a decrease in main stress and shear stress compared to a normal  $\text{Al}_2\text{O}_3/\text{TiC}$  composite.

The friction coefficient between two smooth bodies sliding under elasticity-loaded conditions in an elliptical contact can be expressed as [18]:

$$\mu = A \frac{\tau}{P^{1/3}} \left( \frac{3}{4E'} \right)^{2/3} \quad (2)$$

where  $A$  is a constant determined by contact geometry,  $\tau$  is critical shear stress at the interface, which may be a lubricant film,  $P$  is the normal load, and  $E'$  the effective elastic modulus of the contact materials. For a given contact geometry Eq. (2) shows that the friction coefficient varies linearly with critical

Table 3

Comparison of the maximum main stress and shear stress of AT and ATF2 ceramic composites calculated by finite element method (sliding speed 400 r/min)

Specimen	Maximum main stress (MPa)	Maximum shear stress (MPa)
AT	162	169
ATF2	97	135

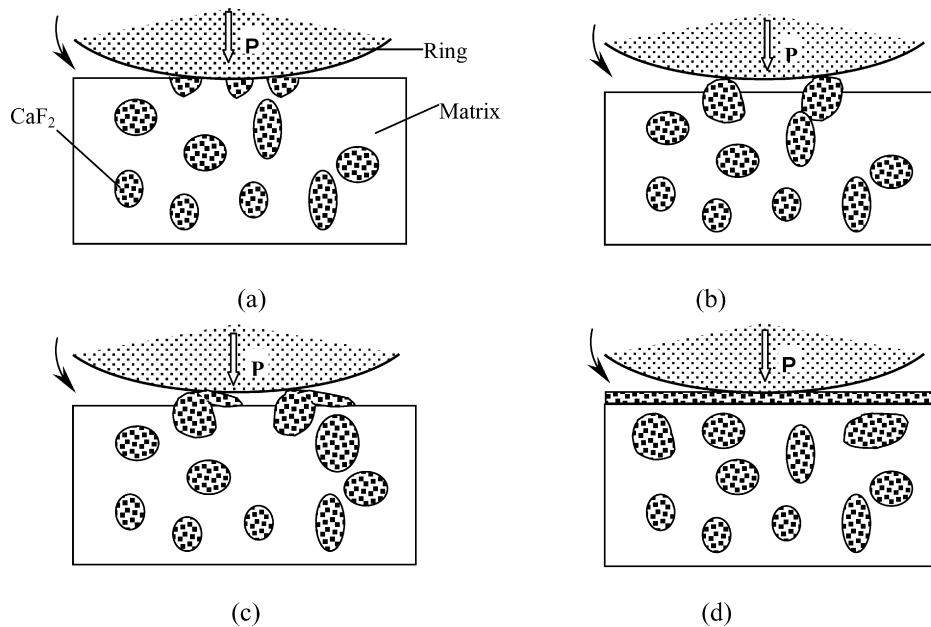


Fig. 10. Schematic diagram of the formation process of self tribofilm between the sliding couple.

shear stress. When there is a tribofilm on the wear surface, the matrix endures the load, and friction occurs on the lubricant film [19,20]. As the lubricant film on the wear surface had a much smaller critical shear stress than the substrate and thus resulted in a reduced friction coefficient according to Eq. (2).

The increase in  $\text{CaF}_2$  content led to a decrease in the coefficient of friction of  $\text{Al}_2\text{O}_3/\text{TiC}/\text{CaF}_2$  ceramic composites sliding against cemented carbide. This may be due to the formation of a  $\text{CaF}_2$  self tribofilm between the sliding couple. Since the  $\text{CaF}_2$  acted as a solid lubricant, the friction coefficient decreased as the  $\text{CaF}_2$  was released and smeared on the wear surface. This self-tribofilm works as a lubricious buffer between cemented carbide ring and the ceramic block in sliding process to significantly reduce the friction coefficient and the wear rate. This means that self-lubrication can be accomplished for  $\text{Al}_2\text{O}_3/\text{TiC}/\text{CaF}_2$  composites when with low  $\text{CaF}_2$  content (less than 10 vol.%).

Fig. 12 shows the SEM micrograph of the worn surface of ATF3 ceramic composite with 15 vol.% proportions of  $\text{CaF}_2$  solid lubricants. In comparison with Fig. 9, it exhibited a damaged surface, a lot of damages could be observed on the tribofilm. The results indicate that  $\text{CaF}_2$  has been released and smeared on the wear surface, and reveals the existence of a broken tribofilm on the worn surface of after sliding wear tests.

Therefore, when the content of  $\text{CaF}_2$  solid lubricants is less than 10 vol.%, the wear rate of  $\text{Al}_2\text{O}_3/\text{TiC}/\text{CaF}_2$  composites decreases with increase in the  $\text{CaF}_2$  content, and this may be due to the formation of a dense self tribofilm between the sliding couple, and to the decrease in main stress and shear stress compared to a normal  $\text{Al}_2\text{O}_3/\text{TiC}$  composite. With further increases in the  $\text{CaF}_2$  content, the wear rate of  $\text{Al}_2\text{O}_3/\text{TiC}/\text{CaF}_2$  composites increases greatly. This is attributed to the large degradation of mechanical properties when with higher  $\text{CaF}_2$  content as can be seen in Table 2, and to the formation of a broken tribofilm between the sliding couple.

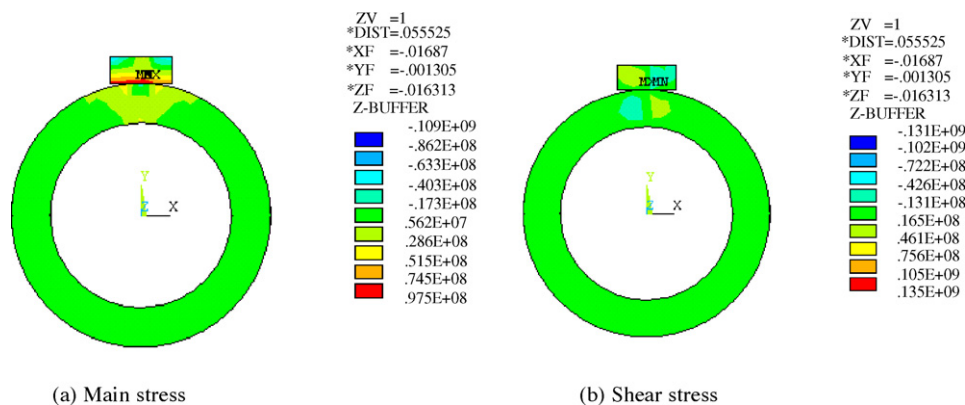


Fig. 11. Stress distribution in the sliding couple (ATF2/YG8) calculated by finite element method (FEM): (a) main stress, and (b) shear stress (sliding speed  $v = 400$  r/min).

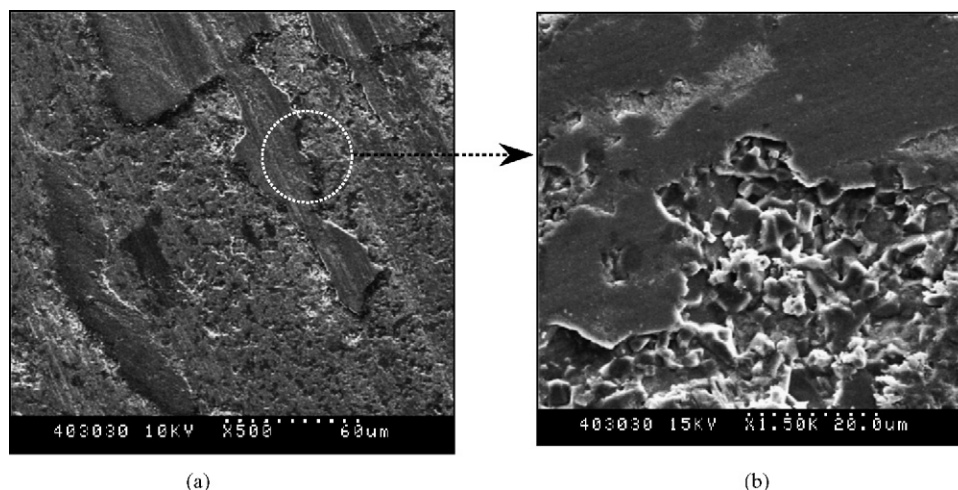


Fig. 12. SEM micrographs of the worn surfaces of (a) ATF3 ( $\text{Al}_2\text{O}_3/\text{TiC}/15 \text{ vol.}\% \text{ CaF}_2$ ) ceramic composite, (b) enlarged SEM micrograph corresponding to (a).

This means that self-lubrication could not be accomplished for  $\text{Al}_2\text{O}_3/\text{TiC}/\text{CaF}_2$  composites when with high  $\text{CaF}_2$  content (more than 10 vol.%).

The results show that tribofilm plays a very important role on the friction and wear behavior of  $\text{Al}_2\text{O}_3/\text{TiC}/\text{CaF}_2$  ceramic composites. Two types of tribofilms are present on the worn surface depending on the  $\text{CaF}_2$  content. Dense tribofilm on the surface can protect the ceramics from severe wear by brittle microfracture, and thus significantly reduces the friction coefficient and wear rate. While broken tribofilm on the surface leads to the increase in friction coefficient and wear rate.

#### 4. Conclusions

$\text{Al}_2\text{O}_3/\text{TiC}$  ceramic composites with the additions of  $\text{CaF}_2$  solid lubricants were produced by hot pressing. Sliding wear tests against cemented carbide were performed on these ceramic composites. Detailed observations and analyses of the wear surface have revealed that two types of tribofilms are present on the worn surface depending on the  $\text{CaF}_2$  content. A dense self tribofilm with a smooth surface associated with small friction coefficient and low wear rate is formed by the releasing and smearing of  $\text{CaF}_2$  solid lubricants on the wear surface when with low  $\text{CaF}_2$  content (less than 10 vol.%). This dense self tribofilm acted as solid lubricant film between the sliding couple, and resulted in small friction coefficient and low wear rate. A broken tribofilm associated with high friction coefficient and large wear rate is formed when with high  $\text{CaF}_2$  content (more than 10 vol.%). The reason is that large degradation of mechanical properties occurred in samples with high  $\text{CaF}_2$  contents

#### Acknowledgements

This work was supported by the National Natural Science Foundation of China (50275088, 50475133), the Excellent Young Teachers Program of MOE (2055), and the Program

for New Century Excellent Talents in University (NCET-04-0622).

#### References

- [1] J.B. Wachtman Jr., Structural Ceramics, Academic Press Inc., London, 1989.
- [2] D.W. Richerson, Modern Ceramic Engineering, Marcel Dekker Inc., New York, 1992.
- [3] S. Jahanmir, Tribology applications of advanced ceramics, Mater. Res. Soc. Symp. Proc., Mater. Res. Soc. 140 (1989) 285–291.
- [4] D. Jianxin, A. Xing, Friction and wear behavior of  $\text{Al}_2\text{O}_3/\text{TiB}_2$  composite against cemented carbide in various atmospheres at elevated temperature, Wear 195 (1996) 128–132.
- [5] B. Prakash, J. Mukerji, S. Kalia, Tribological properties of  $\text{Al}_2\text{O}_3/\text{TiN}$  composites, Am. Ceram. Soc. Bull. 77 (9) (1998) 68–72.
- [6] D. Jianxin, Friction and wear behavior of  $\text{Al}_2\text{O}_3/\text{TiB}_2/\text{SiC}$  ceramic composite at temperature up to 800 °C, Ceram. Int. 27 (2) (2001) 135–141.
- [7] R. Westergard, A. Ahlin, N. Axen, Sliding wear and friction of  $\text{Si}_3\text{N}_4/\text{SiC}$  based ceramic composites containing hexagonal boron nitride, J. Eng. Tribol. 212 (5) (1998) 381–387.
- [8] Y. Wang, F.J. Worzala, A.R. Lefkow, Friction and wear properties of partially stabilized zirconia with solid lubrication, Wear 167 (1993) 23–31.
- [9] D.G. Teer, New solid lubricant coatings, Wear 251 (2001) 1068–1074.
- [10] D. Julthongpiput, H.S. Ahn, A. Sidorenko, D.I. Kim, V.V. Tsukruk, Towards self-lubricated nanocoatings, Tribol. Int. 35 (2002) 829–836.
- [11] J.M. Carrapichano, J.R. Gomes, R.F. Silva, Tribological behavior of  $\text{Si}_3\text{N}_4/\text{BN}$  ceramic materials for dry sliding applications, Wear 253 (9–10) (2002) 1070–1076.
- [12] P.J. Blau, B. Dumont, D.N. Braski, Reciprocating friction and wear behavior of a ceramic-matrix graphite composite for possible use in diesel engine valve guides, Wear 225–229 (1999) 1338–1349.
- [13] T. Aizawa, T. Akhadejdamrong, A. Mitsuo, Self-lubrication of nitride ceramic coating by the chlorine ion implantation, Surf. Coat. Technol. 177–178 (2004) 573–581.
- [14] D. Jianxin, C. Tongkun, L. Lili, Self-lubricating behaviors of  $\text{Al}_2\text{O}_3/\text{TiB}_2$  ceramic tools in dry high-speed machining of hardened steel, J. Eur. Ceram. Soc. 25 (7) (2005) 1073–1079.
- [15] T. Akhadejdamrong, T. Aizawa, M. Yoshitake, A. Mitsuo, T. Yamamoto, Y. Ikuhara, Self-lubrication mechanism of chlorine implanted TiN coatings, Wear 254 (7–8) (2003) 668–679.

- [16] R.F. Cook, B.R. Lawn, A modified indentation toughness technique, *J. Am. Ceram. Soc.* 66 (11) (1983) 200–201.
- [17] W. Shizhu, *Theory of Tribology*, Tsinghua University Press, Beijing, 1990.
- [18] H. Liu, M. Fine, Tribological behavior of SiC whisker/ $\text{Al}_2\text{O}_3$  composites against carburized 8620 steel in lubrication sliding, *J. Am. Ceram. Soc.* 74 (9) (1991) 2224–2233.
- [19] R.A. Page, Development of self-lubricating ceramics using surface and bulk oxidizing species, in: *Advances in Engineering Tribology*, Illinois STLE Publication, 1991.
- [20] T. Aizawa, T. Akhadejdamrong, C. Iwamoto, Y. Ikuhara, A. Mitsuo, Self-lubrication of chlorine-implanted titanium nitride coating, *J. Am. Ceram. Soc.* 85 (1) (2002) 21–24.